Journal of Energy Storage 60 (2023) 106704

Contents lists available at ScienceDirect

Journal of Energy Storage

journal homepage: www.elsevier.com/locate/est

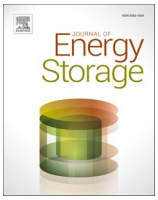

Research papers

Hydrothermal nitrogen doping of anthracene oil-derived activated carbons for wide voltage asymmetric capacitors

Agata Moyseowicz [a], Zoraida González [b,*], Sonia Melendi-Espina [c], Beatriz Acevedo [c], Georgeta Predeanu [d], Sorin M. Axinte [e], Juan J. Fernández [f], Marcos Granda [b], Daria Minta [a], Adam Moyseowicz [a], Grażyna Gryglewicz [a,*]

[a] Department of Process Engineering and Technology of Polymer and Carbon Materials, Wrocław University of Science and Technology, Gdańska 7/9, 50-344 Wrocław, Poland
[b] Instituto de Ciencia y Tecnología del Carbono (INCAR-CSIC), Francisco Pintado Fe26, 33011 Oviedo, Spain
[c] School of Engineering, University of East Anglia, Norwich Research Park, NR4 7TJ Norwich, UK
[d] Faculty of Applied Chemistry and Materials Science, Research Center for Environmental Protection and Eco-friendly Technologies, University Politehnica of Bucharest, 1 Polizu St., 011061 Bucharest, Romania
[e] Claudiu TopRom SRL, Bucharest, Romania
[f] Industrial Química del Nalon, S.A., 33100 Trubia, Spain

ARTICLE INFO

Keywords:
Anthracene oil-derived activated carbon
Aqueous electrolyte
Asymmetric supercapacitor

ABSTRACT

This work focused on the development of doping procedures to introduce nitrogen functionalities on an activated carbon derived from anthracene oil to be subsequently used on wide voltage asymmetric capacitors. For that, ammonia solution was used and different hydrothermal conditions applied. Tailoring the temperature treatment (120 and 180 °C), nitrogen-doped activated carbons (N-ACs) with different nitrogen content (5.6 and 4.1 at. %) and diverse speciation were obtained. N-ACs exhibited excellent capacitive behavior and long-life cycle in a three-electrode cell using KOH aqueous solution as electrolyte. The significant capacitance value of 291 F g^{-1} at 0.2 A g^{-1} was achieved by the N-AC obtained at 180 °C. Furthermore, full carbon asymmetric supercapacitors incorporating N-ACs as negative electrodes were assembled, and an operating voltage window of 1.3 V in 6 M KOH solution established. As a result, high energy densities were achieved in the devices, particularly in that including N-AC-180. Electrochemical tests revealed that pyridinic and quaternary nitrogen species of N-ACs play a critical role in the excellent asymmetric supercapacitor electrochemical performance, including improvement of conductivity and specific capacitance.

1. Introduction

Electrochemical energy storage systems, such as supercapacitors (SCs) and batteries, are daily used to store electrical energy for the electronic devices, such as mobile phones and laptops, along with hybrid and electric vehicles or electric scooters. Due to the growing demand of these appliances, the development of energy storage systems with improved performance is crucial, especially in terms of high specific capacitance, energy/power density values and long-term behavior. According to the charge storage mechanism implied in their operation, SCs are classified into electrical double-layer capacitors (EDLCs) and pseudocapacitors [1,2]. EDLCs have received extensive attention due to their fast energy delivery, high power capability, short charging time, good electrochemical reversibility, and cyclability. The selection of suitable electrode materials and appropriate electrolytes play a critical role in their resulting performance. Particularly, the enhancement of SCs electrochemical behavior can be achieved by introducing redox active functional groups, as well as improving the electrical conductivity of tailored active materials. From the wide variety of carbon materials available, activated carbons (ACs) remain the predominant materials in the manufacture of electrodes for commercial SCs, due to their low cost, easy processability, relatively good electrical conductivity, and high specific surface area [3]. The energy storage mechanism of EDLCs arises from the reversible adsorption/desorption of electrolyte ions at the electrolyte/electrode interface. Thus, the electrochemical performance of EDLCs is strongly related to the porous structure of the electrode

* Corresponding authors.
E-mail addresses: zoraidag@incar.csic.es (Z. González), grazyna.gryglewicz@pwr.edu.pl (G. Gryglewicz).

https://doi.org/10.1016/j.est.2023.106704
Received 27 November 2022; Received in revised form 29 December 2022; Accepted 14 January 2023
Available online 21 January 2023

material, mainly to the BET surface area (S_{BET}) and pore size distribution [4,5]. In this context, the specific capacitance (C_{sp}) of ACs rises almost linearly with the increase of BET surface area up to 2000 m^2 g^{-1}. However, further development of porous structure leads to linearity disturbance around those C_{sp} values [6]. Commercially available ACs are mostly steam-activated materials, showing a typical S_{BET} close to 1000–1500 m^2 g^{-1}. Chemical activation of carbon-based precursors results in highly porous materials, with S_{BET} achieving values of up to 3000 m^2 g^{-1} [7]. However, even though reaching these higher specific surface areas, the C_{sp} of the obtained ACs is still limited [6].

To improve the capacitive properties of carbon-based SCs, the synthesis of ACs using heteroatom-rich precursors along with ACs surface modification via post-treatment with reactive heteroatom sources have been explored. Nitrogen, oxygen and sulfur seem to be the most attractive heteroatoms for ACs doping [8–12]. Specifically, nitrogen enhances the electrochemical performance of carbon materials by locally modifying their hexagonal Csp^2 network and providing electrons for the π electron pair in such aromatic structure. Thus, N-doping of ACs leads to the improvement of their conductivity and wettability, both key parameters in the design of active electrode materials [12,13]. A variety of procedures can be followed to dope ACs with nitrogen functionalities. Several authors have investigated different post-activation treatments. For instance, reaction with ammonia gas (amination), ammonia and air mixtures (ammoxidation) or treatment with nitrogen-containing compounds like melamine and urea [8,14–20]. An alternative route is the use of N-rich carbon precursors, including polymers, such as PAN, PANI, PVP, and chitosan [12,21,22]. Among many reactants containing nitrogen in their structure, ammonia seems to be the most suitable one due to its availability, low cost and high nitrogen content.

Reports on the use of N-doped ACs as active electrode materials for aqueous SCs show capacitance values between 150 and 250 F g^{-1}, depending on the nitrogen content of the AC, the applied current densities and the electrolyte selected [8,12,23–25]. However, in symmetric devices, the relatively high C_{sp} values achieved do not improve to a high extent the energy and power densities. This is due to their narrow operational voltage, which is a significant drawback for the next generation of devices. The theoretical potential of water decomposition (1.23 V) usually results on the limitation of the operating voltage to 1 V. In consequence, the most promising approach to enhance SCs performance is the increasing of operational voltage, which can be achieved by setting up an asymmetric configuration. In that system two electrodes made from different active materials with dissimilar working-range potentials are assembled in the same electrolyte. The complementary potential ranges widen the operating voltage window of the whole device, thus leading to improved energy and power density values [26]. Chen et al. used an AC doped with nitrogen and sulfur as negative electrode in an asymmetric cell operating in 6 M KOH solution as electrolyte at a voltage of 1.2 V, resulting in a specific capacitance value of 84 F g^{-1} at 0.5 A g^{-1} [27]. The asymmetric capacitor with N-doped hierarchical porous carbon nanospheres assembled by Yu et al. [28] operated at a higher voltage (1.6 V) in H_2SO_4 solution, achieving a C_{sp} of 81 F g^{-1} at 1 A g^{-1}.

In the last years, hydrothermal processes have been successfully used as a mild carbonization methodology [29–31]. In addition, they can be considered as a suitable route for N-doping of carbon-based materials. However, there are only few reports employing hydrothermal approaches for nitrogen (or other heteroatoms) enrichment of pristine ACs [32].

In the present work, we propose the facile and scalable synthesis of N-doped ACs by hydrothermal treatment in presence of ammonia solution, as a promising functionalization method under mild conditions. Various reaction temperatures led to the incorporation of a wide range of nitrogen moieties in N-ACs, while preserving the porous structure of the pristine AC. Hydrothermal N-doped ACs with a nitrogen content up to 5.6 at. % were investigated as electrode materials for SCs in a three-electrode system. The highest specific capacitance value of 291 F g^{-1} at 0.2 A g^{-1} was achieved for N-AC-180 with 4.1 at. % of N. N-AC-180 showed an excellent rate capability and long-term performance. Furthermore, N-ACs were used as negative electrode in a full-carbon asymmetric device. The high capacitance value and wide operational voltage window (1.3 V) of the device with N-AC-180 as negative electrode resulted in an energy density of 11.3 Wh kg^{-1} at a power density of 163 W kg^{-1}. Furthermore, this asymmetric device displays an exceptional energy density of 7.9 Wh kg^{-1} at a high-power density of 10 kW kg^{-1}.

2. Experimental section

2.1. Synthesis of materials

An AC was prepared from a green coke, which was obtained in turn from anthracene oil. The green coke was chemically activated using KOH as activating agent [34]. 0.2 g of AC was subsequently mixed with 200 mL of ammonia solution (12.5 % v/v). The mixture was hydrothermally treated in a stainless-steel autoclave at 120 and 180 °C for 5 h. After the reaction time, the autoclave was cooled down to room temperature. The resulting N-ACs (N-AC-120 and N-AC-180) were centrifuged and afterward washed with deionized water several times until neutral pH. Finally, the samples were dried in a vacuum oven at 60 °C overnight.

A mesophase pitch-based activated carbon (PAC) was prepared from coal-tar pitch by carbonization followed by chemical activation with KOH and used as positive electrode in the asymmetric SCs configurations.

2.2. Structural and chemical characterization of the synthesized materials

The porous texture of the materials was determined by means of N_2 adsorption at 77 K using an Autosorb IQ gas sorption analyzer (Quantachrome). The quenched solid density functional theory (QSDFT) was used to determine pore size distribution. X-ray photoelectron spectroscopy (XPS) measurements were carried out with a Kratos Axis Ultra-DLD, K-Alpha+ instrument. The surface atomic concentrations were calculated from the ratio of the corresponding peak areas after correction with theoretical sensitivity factors based on the Scofield's photoionization cross-sections. The curve fitting of the high resolution N1s core-level spectra was performed using the CasaXPS software after a Shirley background subtraction. Peak fitting was performed using a Gaussian-Lorentzian (70/30) peak shape. The N 1 s core level spectra of the N-doped samples were fitted with five components, corresponding to pyridinic-N (N-6, 398.7 ± 0.3 eV), amides/imides or lactams (N—C, 399.7 ± 0.2 eV), pyrrolic-N and -NH_2 (N-5, 400.3 ± 0.3 eV), quaternary-N (N-Q, 401.4 ± 0.5 eV), and pyridine N-oxides (N-X, 402–405 eV) [33]. The elemental determination of the C, H and N contents was investigated using a Vario MICRO cube analyzer, and the oxygen content was directly measured by means of a Carlo Erba EA 1108 Elemental Analyzer. The Raman spectra were recorded on the Bruker dispersive Raman Spectrometer Senterra coupled with a confocal microscope with 532 nm laser. The spectral data were collected and further processed using the Bruker OPUS software.

2.3. Electrodes assembly and electrochemical testing

Pellet-type electrodes, with a geometric surface area of 0.64 cm^2, were prepared by mixing 85 wt% of the synthesized active material (AC, N-AC-120, N-AC-180), 5 wt% of acetylene carbon black as conductive agent (CB), and 10 wt% of polyvinylidene fluoride as binder (PVDF, Kynar Flex 2801). The mass and thickness of the electrodes were approximately 8 mg and 150 μm, respectively. Three-electrode configurations were assembled in a T-type Swagelok® cell using the previously mentioned materials as working electrodes (WE), a Hg|HgO as a reference electrode (RE) and PAC as the counter electrode (CE). The WE and

CE were separated by a glassy fibrous paper and a 6 M KOH aqueous solution was used as electrolyte. Gold current collectors were used to avoid corrosion and to preserve comparable experimental conditions. The electrochemical performance of the different ACs was evaluated by means of cyclic voltammetry (CV, at scan rates ranging between 1 and 100 mv s^{-1}) and galvanostatic charge/discharge (GCD, at current densities from 0.2 to 20 A g^{-1}) experiments, using a potentiostat-galvanostat supplied by VSP Biologic (France). The specific capacitance values (C_{sp}, F g^{-1}) were calculated from both the cyclic voltammograms (CVs) and the galvanostatic discharge profiles according to Eqs. (1) and (2), respectively.

$$C_{sp} = \frac{\int Idt}{\nu m_{el}} \tag{1}$$

$$C_{sp} = \frac{\int Idt}{U m_{el}} \tag{2}$$

where I is the current measured or applied (A), t is the time (s), ν is the scan rate (V s^{-1}), U is the operational voltage window (V), and m_{el} is the mass of the active material in the corresponding electrode (g).

Electrochemical impedance spectroscopy (EIS) measurements were also performed under open circuit potential in a frequency range from 100 kHz to 10 mHz at an amplitude of 5 mV. The imaginary $C''(\omega)$ part of the capacitance (F g^{-1}) as the function of frequency was calculated according to the Eq. (3) [34]:

$$C''(\omega) = \frac{Z'(\omega)}{m\omega|Z(\omega)|^2} \tag{3}$$

where $Z'(\omega)$ is the real part of the impedance, $Z(\omega)$ is the total impedance and m is the mass of WE. The cyclability was determined using GCD measurements at a current density of 1 A g^{-1}.

The full carbon asymmetric SCs to be evaluated were set up utilizing N-ACs (or AC for comparative purposes) and PAC, as negative and positive electrodes respectively, and separated by a glassy fibrous separator. The resulting devices were labelled as AC|PAC and N-ACs|PAC. The mass ratio of the negative electrode to the positive one was fixed to 1:1. The preliminary electrochemical measurements were carried out in a 2-electrode cell configuration (CV and GCD) and conducted at increasing voltage windows (from 0 to 1.0–1.4 V) with a 0.1 V step. The cyclability tests were performed by GCD measurements at an applied current density of 1 A g^{-1}.

The stored specific energy (E in Wh kg^{-1}) and specific power delivered (P in kW kg^{-1}) were calculated using Eqs. (4) and (5), respectively [35]:

$$\mathrm{E} = \frac{1}{2}\mathrm{CU}^2 \tag{4}$$

$$P = \frac{E}{t} \tag{5}$$

3. Results and discussion

3.1. Characterization of the active materials

Hydrothermal treatment of AC in ammonia solution at various temperatures successfully resulted in N-doped ACs with comparable textural parameters. N_2 adsorption-desorption isotherms at 77 K of the pristine AC and the derived nitrogen doped materials are shown in Fig. 1a. All the isotherms are classified as Type I, as defined by IUPAC [36], indicating the samples under study are mainly microporous. Hydrothermal ammonia treatment of AC slightly reduced porous structure by, approximately, 10 % (Table 1). As a result, the BET specific surface area of AC before N-doping is 2306 m^2 g^{-1} and decreases to 2080 and 2065 m^2 g^{-1} for N-AC-120 and N-AC-180, respectively. Pores with 0.7–1 nm width are predominant in all samples (Fig. 1b). N-doped ACs show a comparable porous structure, maintaining the microporous nature of the pristine AC. The total pore volume (V_T) of the N-ACs is in the range of 0.877–0.902 cm^3/g with a similar contribution of micropores, V_{DR}/V_T (0.77–0.80). Due to the doping, the average micropore size (L_0) of N-ACs decreases in comparison to the pristine AC (1.02–1.06 nm vs. 1.14 nm, respectively).

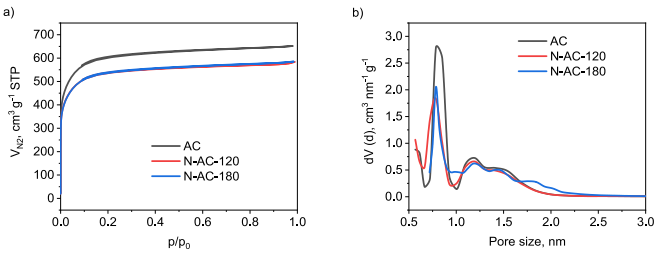

Fig. 1. N_2 adsorption-desorption isotherms at 77 K (a) and QSDFT pore size distribution (b) for AC and N-ACs.

Table 1
Textural parameters of AC and N-ACs.

Material	S_{BET} (m^2 g^{-1})	V_T (cm^3/g)	V_{DR} (cm^3/g)	V_{DR}/V_T	L_0 (nm)
AC	2306	1.006	0.802	0.80	1.14
N-AC-120	2080	0.887	0.712	0.80	1.06
N-AC-180	2065	0.902	0.699	0.77	1.03

The morphology of the different materials was investigated by means of FESEM (Fig. 2). According to the images obtained, the size of AC and N-ACs particles does not exceed 2 μm (Fig. 2). The morphology of N-AC-120 is comparable to that of pristine AC, nevertheless there are significant differences when N-AC-180 is considered. This sample seems to have significantly larger particles, which may be due to the increased autogenic pressure experienced (8.8 bars at 180 °C), corroborating previously reported results [37]. High-magnification images of N-AC-120 and N-AC-180 illustrate that their morphology is comparable. Surfaces do not show any roughness, as in the case of the pristine AC.

The survey spectra of the pristine AC and N-ACs as well as the distribution of nitrogen species were investigated by XPS (Fig. 3). Hydrothermal treatment with ammonia at 120 °C successfully introduces nitrogen into the AC structure, up to 5.6 at. % (Table 2). However, amination at higher temperature (180 °C) leads to a decrease in the nitrogen content (4.1 at. %). The nitrogen content of N-AC-120 and N-AC-180 determined by elemental analysis is 5.9 and 4.3 wt% respectively, suggesting the uniform distribution of nitrogen species in the samples. As expected, the enrichment in nitrogen is accompanied by a decrease in oxygen content (from 9.4 vs 6.2–6.1 at. %, Table 2).

The curve fitting to determine the nature of the nitrogenated functional groups introduced after the hydrothermal treatment is shown in Fig. 3b-c. Pyridinic-N (N-6) groups exhibit the highest contribution to the total nitrogen content in both N-ACs, being 38 and 47 % in N-AC-120 and N-AC-180 respectively (Table 2). The contribution of N—C (amide/imide/lactams) functional groups in the doped ACs is very similar (19–20 %), regardless of reaction temperature. An increase in the hydrothermal treatment temperature causes a significant decrease in the pyrrolic-N and -NH_2 (N-5) groups, from 22 (N-AC-120) to 11 % (N-AC-180). A similar trend has been reported by Gao et al. [38]. N-AC-180 shows a higher content of N-Q groups (17 %) than N-AC-120 (12.8 %). These findings indicate that N-5 and N—C species undergo transition towards more stable N-6 and N-Q nitrogen functionalities with increasing hydrothermal temperature [39,40].

The carbon inner structure of AC and N-ACs was further examined by means of Raman spectroscopy. The resulting spectra exhibit two typical bands at approximately 1350 and 1590 cm-1, corresponding to the D and G modes, which characterize the structural defects and the graphitic

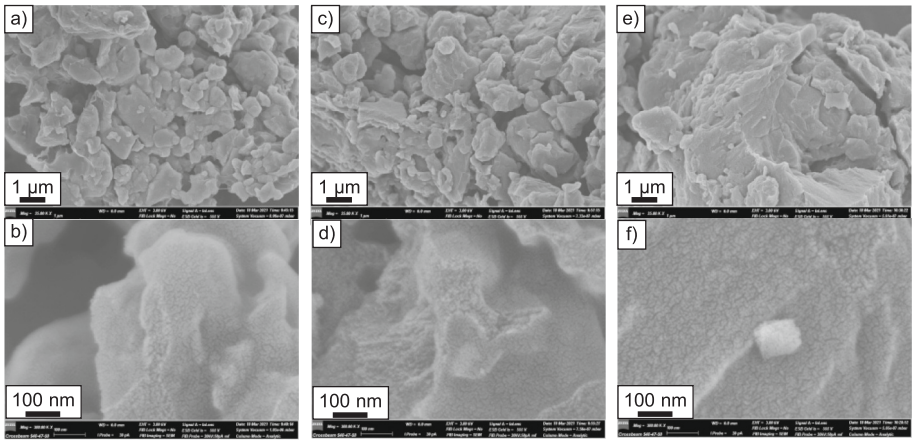

Fig. 2. FESEM images of AC (a, b), N-AC-120 (c, d) and N-AC-180 (e, f).

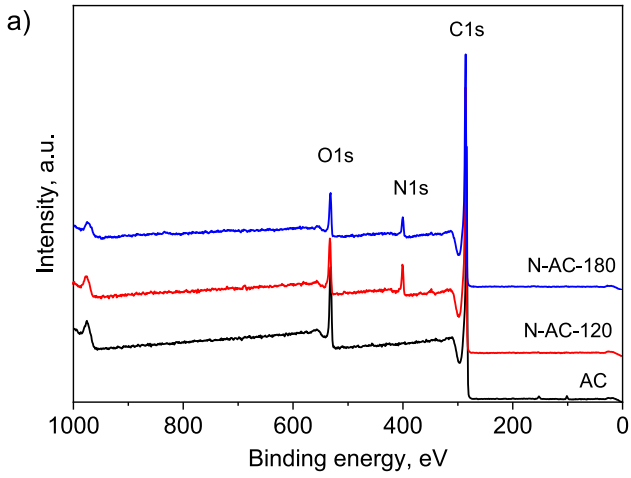

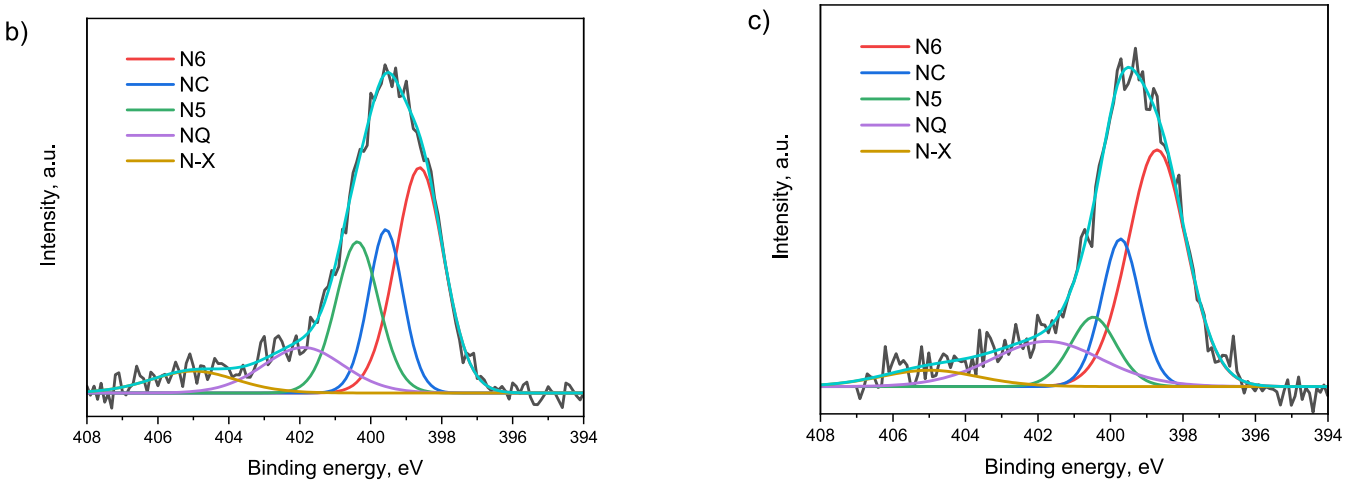

Fig. 3. XPS survey (a) and curve fitted N 1 s spectra of N-AC-120 (b) and N-AC-180 (c).

domains, respectively (**Fig. S1**, Supplementary Information). The intensity ratio of the D to G bands (I_D/I_G) can be associated to a measure of defect density in the carbon structure. There are small differences in the I_D/I_G ratio of the initial AC and N-ACs, being in the range from 0.95 to 1.00. However, it is worth mentioning the influence of the introduced nitrogen on the number of defects and imperfections within the carbon

Table 2
Surface elemental composition determined by XPS and relative abundance (%) of nitrogenated functional groups.

Sample	C at.%	O at.%	N at.%	N 1s curve fitting, %				
				N-6	N-C	N-5	N-Q	N-X
AC	90.6	9.4	–					
N-AC-120	88.2	6.2	5.6	38	20	22	13	7
N-AC-180	89.8	6.1	4.1	47	19	11	17	6

structure, which clearly affects the I_D/I_G value. The increased number of defects in the carbon material after hydrothermal treatment with ammonia at lower temperature is more pronounced. The higher I_D/I_G ratio (1.00) of N-AC-120 can be directly attributed to the greater nitrogen content introduced within the structure in comparison to N-AC-180 (Table 2), whose I_D/I_G ratio was 0.97.

3.2. Electrochemical performance of the materials as electrodes in SCs

N-AC-120 and N-AC-180 were assessed as active electrode materials

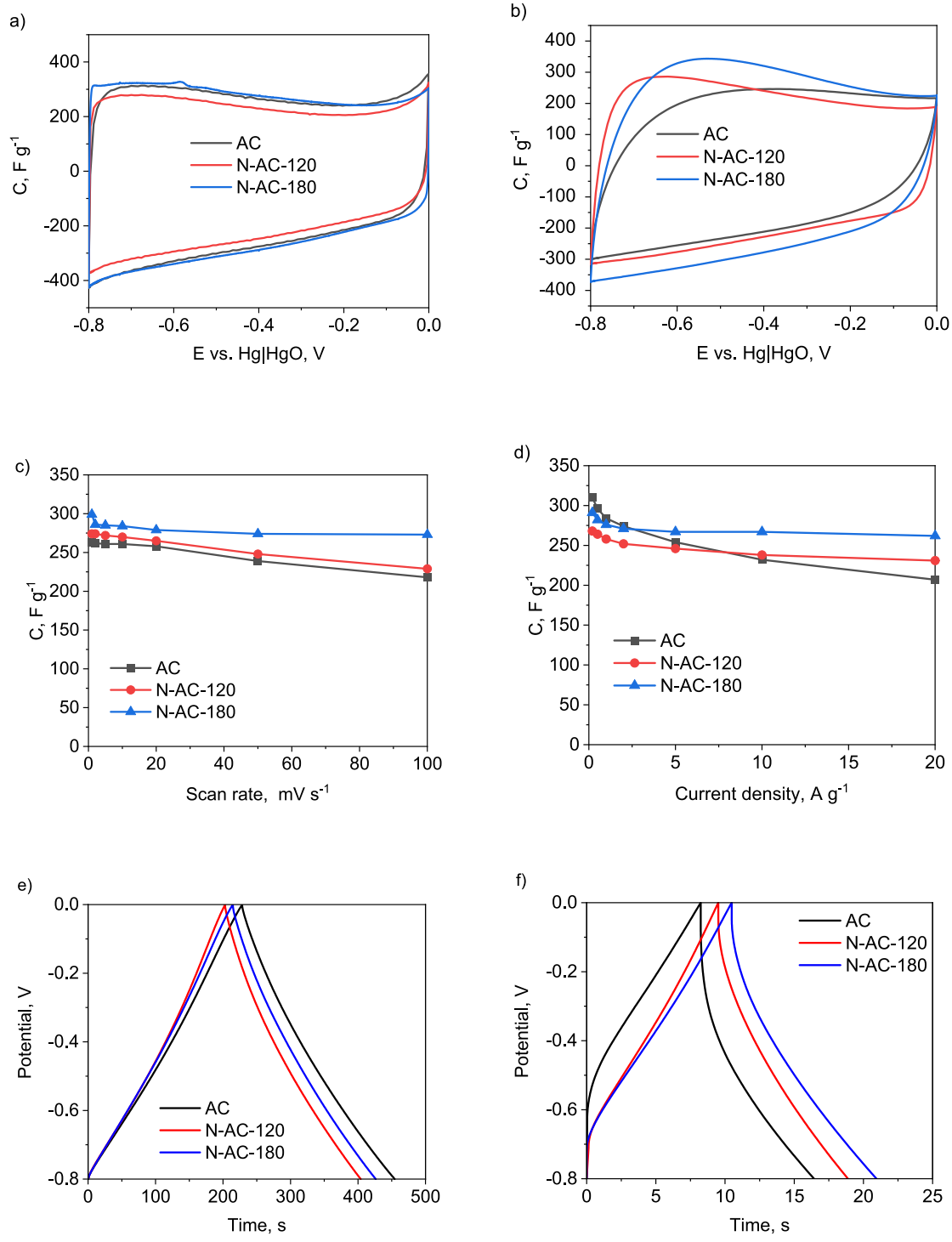

Fig. 4. CVs recorded on the different electrodes at 2 (a) and 100 mV s^{-1} (b) and specific capacitance as a function of the scan rate (c) and the discharge current (d), GCD profiles recorded of starting and N-doped ACs at 1 (e) and 20 A g^{-1} (f) of applied current density.

for SC applications. The capacitive behavior of the starting AC was also studied for comparative purposes. Firstly, the electrochemical performance of the three samples was evaluated in a three-electrode cell configuration with 6 mol L^{-1} KOH as electrolyte.

CV measurements were carried out to obtain preliminary results on the charge storage capability of the N-ACs (Fig. 4). At a low scan rate (2 mV s^{-1}), their corresponding CVs are comparable to that of the pristine AC (Fig. 4a**)**. However, an improved capacitive behavior of the N-ACs is observed at higher scan rates (100 mV s^{-1}) (Fig. 4b). This enhancement relates to the introduction of nitrogen species into their structure, which positively influences their electrical conductivity and charge propagation. Independently of the scan rate or the current density applied, and despite of its higher specific surface area (S_{BET} ~ 2306 vs 2080 and 2065 m^2 g^{-1}, Table 1), the specific capacitance value of the AC electrode is the lowest among all the tested materials (Figs. 4c and d). This result indicates the beneficial impact of nitrogen doping.

Differences found in the capacitive behavior of N-ACs are mainly due to the varied nitrogen content and type/distribution of functional groups introduced into their structure. The resultant N-ACs show comparable BET surface areas, approximately 2000 m^2 g^{-1}, and surface oxygen content (6.1–6.2 at. %) regardless of the temperature selected for the hydrothermal treatment. Moreover, their enhanced electrical conductivity is also related to the presence of nitrogen. Particularly, the best charge propagation is observed on the N-AC-180 electrode, which may be associated to the higher content of N-Q (17 vs 13 %, Table 2). According to theoretical calculations, nitrogen incorporation into the quaternary position causes the appearance of a new donor state near the Fermi level, and hence the doped material presents n-type conductivity [41].

At low current densities (0.2 A g^{-1}), and despite its highest nitrogen doping (5.6 at. %), N-AC-120 exhibits lower capacitance value (283 F g^{-1}) than AC (310 F g^{-1}) and N-AC-180

(291 F g^{-1}) (Fig. 4d**)**. However, at increasing loading current density (up to 20 A g^{-1}), the trend noticeably changes. It can be observed in Fig. 4d that AC C_{sp} continuously decreases, reaching a value of 207 F g^{-1} at the highest current density applied, while the N-doped electrodes display stable and higher values (231 and 267 F g^{-1} at 20 A g^{-1} for N-AC-120 and N-AC-180, respectively). These results prove that hydrothermal treatment is an easy methodology to introduce nitrogen groups into the AC structure, yielding active materials with enhanced electrochemical performance as electrodes in SCs. Additionally, hydrothermal treatment of AC preserves the textural properties of N-rich and highly porous materials.

Fig. 4e and f presents the galvanostatic charge/discharge profiles recorded on the AC and N-AC electrodes. All ACs under evaluation exhibit nearly the typical triangle shaped profile, with a good symmetry between charge and discharge processes and a linear increase/decrease in voltage with time at low current density values (1 A g^{-1}, Fig. 4e). However, clear differences appear at higher current density (20 A g^{-1}, Fig. 4f**)**. The longer charge and discharge times measured on the N-AC-180 electrode (both 10.5 s) corroborate the positive contribution of the N-6 and N-Q functional groups to its improved capacitive performance.

Investigations on the kinetics of ion and charge transport were performed using electrochemical impedance spectroscopy. N-AC-180 electrode shows a markedly lower bulk resistance (0.11 Ω) than N-AC-120 (0.22 Ω) and AC (0.18 Ω) (Fig. 5a). These values include the inherent resistance of the electrolyte and the current collector [42,43]. The charge-transfer resistance (*Rct*) related to the electron transfer step at the electrode/electrolyte interface has been calculated from the diameter of the semicircle developed at the high frequency region. It is worth noting that *Rct* is lower for the N-ACs (17 and 15 mΩ for N-AC-120 and N-AC-180, respectively) than for the starting AC (33 mΩ). According to the literature, monovalent functional groups such as – NH_2 could change C hybridization from sp^2 to sp^3 state, thus interfering with the conjugated π system [44]. This fact could explain the intrinsic resistance in N-AC-120 as it presents a higher N-5 percentage. On the other hand, N-AC-180 exhibits a nearly vertical slope in the low frequency region, which could be ascribed to its enhanced electron transfer rate, a small ion

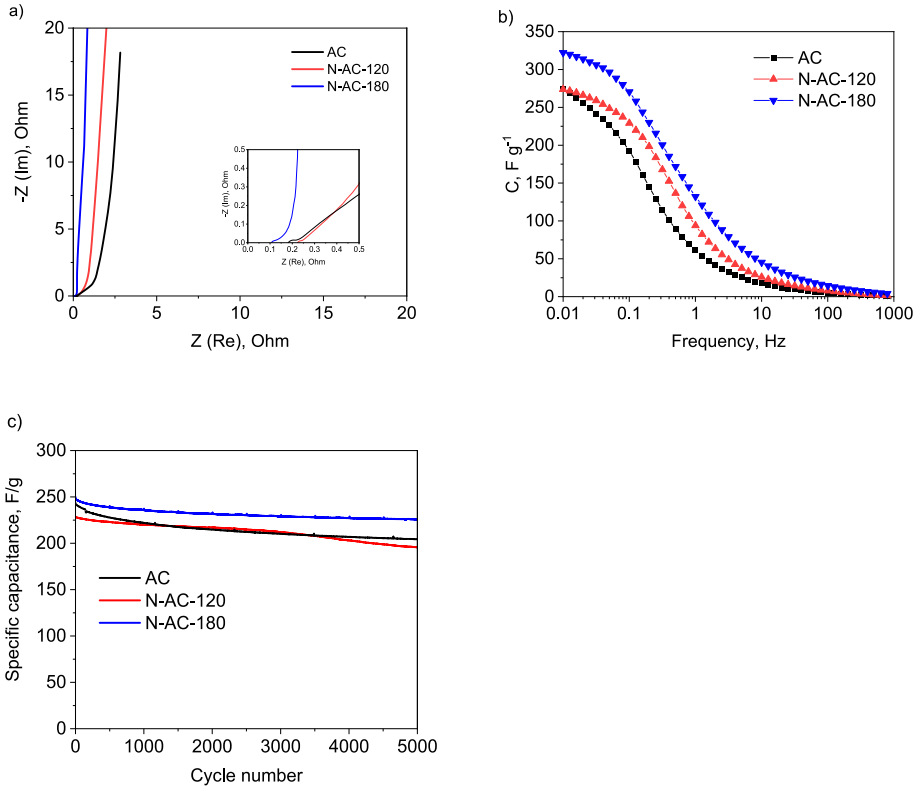

Fig. 5. Nyquist plots recorded on the different electrodes under evaluation (Insert: high frequency region) (a) and specific capacitance as a function of frequency (b) and long-term behavior of AC and N-ACs at 1 A g^{-1} (c).

diffusion resistance, and, subsequently, an improved capacitive behavior of this active electrode material [42]. Based on these results, the specific capacitance vs. frequency for N-ACs and AC is presented in Fig. 5b. N-AC-180 capacitance is higher (289 F g^{-1} at 50 mHz) than that of N-AC-120 and the pristine AC (248 and 227 F g^{-1} at 50 mHz, respectively). At increasing frequency values, the ion diffusion restrictions in the pores are more pronounced for the undoped AC, thus resulting in a marked decrease of the corresponding capacitance value in comparison to N-ACs [45].

Fig. 5c presents the long-term performance of the fabricated electrodes after 5000 charge-discharge cycles at a current density of 1 A g^{-1}. As it can be seen, the higher capacitance value of N-AC-180 is maintained throughout the cycling range. After 5000 cycles this value only decreases from 249 F g^{-1} to 226 F g^{-1}, demonstrating the highest rate capability (91 %). The cyclability tests carried out on the N-ACs electrodes reveal that specific nitrogenated functionalities play a crucial role in their electrochemical performance. These active materials significantly benefit from the quantum capacitance related to the pyridinic and quaternary nitrogen moieties [46].

Further research was conducted using a full carbon asymmetric supercapacitor, setting up N-ACs as negative active electrode materials of the device. The main aim of this asymmetric configuration was to overcome the theoretical potential of water decomposition, thus achieving a wider operational voltage of the SC and, subsequently, higher energy and power density values of the whole system. The CVs recorded at wider voltage windows (1.0 to 1.4 V) are summarized in Fig. 6.

At operating voltages above the theoretical value for water decomposition (1.23 V), the asymmetric SC containing N-AC-120 as negative electrode reveals a more limited capacitive performance than the device including AC or N-AC-180. This may be related to the appearance of high resistivity and inhibition of charge propagation when reaching the mentioned voltage value [47,48]. N-AC-180|PAC maintains an appropriate electrochemical performance even at 1.3 V. These results corroborate those obtained from the preliminary characterization of the materials under evaluation in the three-electrode cell, and therefore confirm the beneficial impact of the surface chemistry, including distribution of nitrogen functionalities, especially N-6 and N-Q, on the charge storage capability of the device. The overall electrochemical performance of all asymmetric SCs significantly dropped down at an operating voltage of 1.4 V.

Fig. 7a shows the evolution of devices specific capacitance with the number of charge/discharge cycles at increasing operational voltage values. As expected, the best cyclability and the highest rate capability (89 % after 4000 cycles) is revealed for N-AC-180|PAC. This is mainly due to the presence of quaternary nitrogen in its inner structure, thus improving the electron transfer kinetics [23]. The asymmetric device with N-AC-180 as negative electrode also shows enhanced operating parameters, such as specific capacitance and long-term performance, in comparison to the other two systems assessed. Furthermore, the higher capacitance and wider operational voltage result in improved energy and power density values, as it can be seen in the Ragone plots (Fig. 7b and **Fig. S2-Supporting Information**). N-AC-180|PAC device exhibits the highest energy density (11.6 Wh kg^{-1} at a power density of 163 W kg^{-1}). At increased power densities, the good capacitive performance of this device is maintained along with its excellent energy density, achieving a value of 7.9 Wh kg^{-1} at a power density of 10 kW kg^{-1}. N-AC-180|PAC device stands out among other full carbon electrochemical capacitors operating in an alkaline electrolyte due to the high capacitive properties of the N-doped AC and wide operating voltage of 1.3 V (KOH electrolyte). The summary of the electrochemical performance of several full carbon SCs is presented in **Table S1** (Supplementary Information).

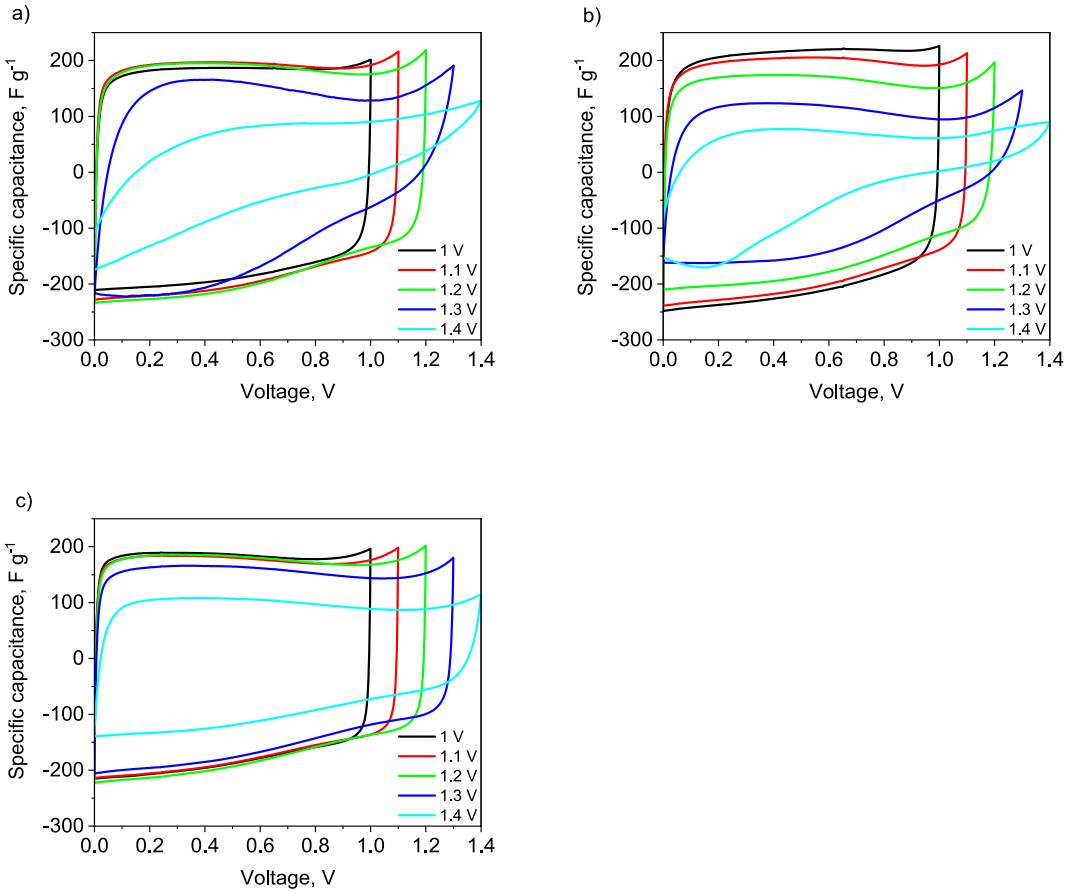

Fig. 6. CVs recorded on the asymmetric SCs AC|PAC (a), N-AC-120|PAC (b), and N-AC-180|PAC (c) at various operational voltage windows (v_{scan} = 10 mV s^{-1}).

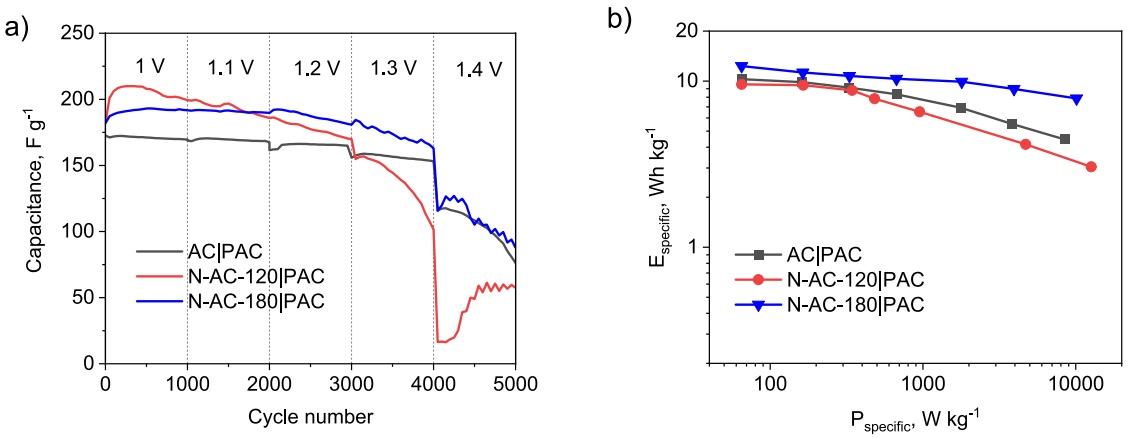

Fig. 7. Long-term performance of asymmetric devices measured, by applying 1 A g^{-1}, at increasing operational voltage values (a) and the corresponding Ragone plots recorded at 1.3 V (b).

4. Conclusions

N-doped ACs were successfully obtained via hydrothermal ammonia treatment of an AC at different temperatures (120 and 180 °C). Depending on the temperature selected, the amount of surface nitrogen content incorporated was in the range 4.1–5.6 at. %. The BET surface area of the N-ACs was between 2065 and 2080 m^2 g^{-1}, being at around 10 % lower than that of the pristine AC. However, N-AC-120 and N-AC-180 showed better capacitive performance measured in a three-electrode cell configuration, achieving 231 and 267 F g^{-1} at a high current density (20 A g^{-1}) compared to undoped AC. The asymmetric device prepared with N-AC-180 as the negative electrode and a PAC as the positive one (N-AC-180|PAC) was able to operate in a wide voltage window of 1.3 V, using an aqueous KOH electrolyte, and maintained 89 % of the initial capacitance after 4000 charge-discharge cycles. The N-AC-180|PAC capacitor exhibited an energy density of 7.9 Wh kg^{-1} at a power density of 10 kW kg^{-1}, and it is therefore suitable for high-power applications. The excellent electrochemical performance of the assembled asymmetric capacitor was due to the developed structure of N-AC-180, improved surface wettability due to nitrogenated structure, and enhanced electrical conductivity as a result of the appropriate nitrogen doping.

CRediT authorship contribution statement

Agata Moyseowicz: Conceptualization, Methodology, Investigation, Writing – original draft, Visualization. **Zoraida González:** Formal analysis, Supervision, Writing – original draft. **Sonia Melendi-Espina:** Supervision, Formal analysis, Funding acquisition, Writing – original draft. **Beatriz Acevedo:** Investigation, Writing – review & editing. **Georgeta Predeanu:** Funding acquisition, Writing – review & editing. **Sorin M. Axinte:** Funding acquisition, Writing – review & editing. **Juan J. Fernández:** Funding acquisition, Writing – review & editing. **Marcos Granda:** Supervision, Funding acquisition, Writing – review & editing. **Daria Minta:** Investigation. **Adam Moyseowicz:** Investigation, Writing – review & editing. **Grażyna Gryglewicz:** Conceptualization, Supervision, Funding acquisition, Writing – review & editing.

Declaration of competing interest

The authors declare the following financial interests/personal relationships which may be considered as potential competing interests: Grazyna Gryglewicz reports financial support was provided by European Union's Research Fund for Coal and Steel (RFCS).

Data availability

Data will be made available on request.

Acknowledgements

The research leading to these results has received funding from the European Union's Research Fund for Coal and Steel (RFCS) research programme under grant agreement RFCR-CT-2015-00006.

Appendix A. Supplementary data

Supplementary data to this article can be found online at https://doi.org/10.1016/j.est.2023.106704.

References

[1] P. Simon, Y. Gogotsi, Materials for electrochemical capacitors, Nature Materials 7 (2008) 845–854, https://doi.org/10.1038/nmat2297, 2008 7:11.
[2] B.E. Conway, Electrochemical Supercapacitors: Scientific Fundamentals and Technological Applications, Springer, New York, 1999.
[3] A.G. Pandolfo, A.F. Hollenkamp, Carbon properties and their role in supercapacitors, J. Power Sources 157 (2006) 11–27, https://doi.org/10.1016/j.jpowsour.2006.02.065.
[4] J. Yan, Q. Wang, T. Wei, Z. Fan, Recent advances in design and fabrication of electrochemical supercapacitors with high energy densities, Adv. Energy Mater. 4 (2014), 1300816, https://doi.org/10.1002/aenm.201300816.
[5] K. Ideta, D.W. Kim, T. Kim, K. Nakabayashi, J. Miyawaki, J.Il Park, S.H. Yoon, Effect of pore size in activated carbon on the response characteristic of electric double layer capacitor, Journal of Industrial and Engineering Chemistry 102 (2021) 321–326, https://doi.org/10.1016/j.jiec.2021.07.014.
[6] K. Kierzek, G. Gryglewicz, Activated carbons and their evaluation in electric double layer capacitors, Molecules 25 (2020) 4255, https://doi.org/10.3390/molecules25184255.
[7] K. Kierzek, E. Frackowiak, G. Lota, G. Gryglewicz, J. Machnikowski, Electrochemical capacitors based on highly porous carbons prepared by KOH activation, Electrochim. Acta 49 (2004) 515–523, https://doi.org/10.1016/j.electacta.2003.08.026.
[8] B. Li, F. Dai, Q. Xiao, L. Yang, J. Shen, C. Zhang, M. Cai, Nitrogen-doped activated carbon for a high energy hybrid supercapacitor, Energy Environ. Sci. 9 (2016) 102, https://doi.org/10.1039/c5ee03149d.
[9] M.A. Hegazy, M.M. Mohammedy, A.S. Dhmees, Phosphorous and sulfur doped asphaltene derived activated carbon for supercapacitor application, J Energy Storage. 44 (2021), 103331, https://doi.org/10.1016/j.est.2021.103331.
[10] S. Shaheen Shah, S.M. Abu Nayem, N. Sultana, A.J. Saleh Ahammad, M. Abdul Aziz, Preparation of sulfur-doped carbon for supercapacitor applications: a review, ChemSusChem. 2022 (2021) 202101282–202101283, https://doi.org/10.1002/cssc.202101282.
[11] F.R.Maria Sundar Raj, N.V. Jaya, G. Boopathi, D. Kalpana, A. Pandurangan, S-doped activated mesoporous carbon derived from the Borassus flabellifer flower as active electrodes for supercapacitors, Mater, Chem Phys. 240 (2020), 122151, https://doi.org/10.1016/j.matchemphys.2019.122151.
[12] A. Śliwak, N. Díez, E. Miniach, G. Gryglewicz, Nitrogen-containing chitosan-based carbon as an electrode material for high-performance supercapacitors, J. Appl. Electrochem. 46 (2016) 667–677, https://doi.org/10.1007/s10800-016-0955-z.

[13] P. Treeweranuwat, P. Boonyoung, M. Chareonpanich, K. Nueangnoraj, Role of nitrogen on the porosity, surface, and electrochemical characteristics of activated carbon, ACS Omega. 5 (2020) 1911–1918, https://doi.org/10.1021/acsomega.9b03586.
[14] U. Świetlik, B. Grzyb, K. Torchała, G. Gryglewicz, J. Machnikowski, High temperature ammonia treatment of pitch particulates and fibers for nitrogen enriched microporous carbons, Fuel Process. Technol. 119 (2014) 211–217, https://doi.org/10.1016/j.fuproc.2013.11.009.
[15] J. Przepiórski, M. Skrodzewicz, A.W. Morawski, High temperature ammonia treatment of activated carbon for enhancement of CO2 adsorption, Appl. Surf. Sci. 225 (2004) 235–242, https://doi.org/10.1016/j.apsusc.2003.10.006.
[16] R.J.J. Jansen, H. van Bekkum, Amination and ammoxidation of activated carbons, Carbon 32 (1994) 1507–1516, https://doi.org/10.1016/0008-6223(94)90146-5.
[17] N.D. Kim, W. Kim, J.B. Joo, S. Oh, P. Kim, Y. Kim, J. Yi, Electrochemical capacitor performance of N-doped mesoporous carbons prepared by ammoxidation, J. Power Sources 180 (2008) 671–675, https://doi.org/10.1016/j.jpowsour.2008.01.055.
[18] M. Seredych, D. Hulicova-Jurcakova, G.Q. Lu, T.J. Bandosz, Surface functional groups of carbons and the effects of their chemical character, density and accessibility to ions on electrochemical performance, Carbon 46 (2008) 1475–1488, https://doi.org/10.1016/j.carbon.2008.06.027.
[19] M.X. Zhan, Y.W. Liu, W.W. Ye, T. Chen, W.T. Jiao, Modification of activated carbon using urea to enhance the adsorption of dioxins, Environ. Res. 204 (2022), 112035, https://doi.org/10.1016/j.envres.2021.112035.
[20] Y. Wang, H. Xuan, G. Lin, F. Wang, Z. Chen, X. Dong, A melamine-assisted chemical blowing synthesis of N-doped activated carbon sheets for supercapacitor application, J. Power Sources 319 (2016) 262–270, https://doi.org/10.1016/j.jpowsour.2016.04.069.
[21] K. Torchała, K. Kierzek, G. Gryglewicz, J. Machnikowski, Narrow-porous pitch-based carbon fibers of superior capacitance properties in aqueous electrolytes, Electrochim. Acta 167 (2015) 348–356, https://doi.org/10.1016/j.electacta.2015.03.153.
[22] N. Kostoglou, C. Koczwara, S. Stock, C. Tampaxis, G. Charalambopoulou, T. Steriotis, O. Paris, C. Rebholz, C. Mitterer, Nanoporous polymer-derived activated carbon for hydrogen adsorption and electrochemical energy storage, Chem. Eng. J. 427 (2022), 131730, https://doi.org/10.1016/j.cej.2021.131730.
[23] A. Ilnicka M. Skorupska M. Szkoda Z. Zarach P. Kamedulski W. Zielinski J.P. Lukaszewicz , Combined effect of nitrogen-doped functional groups and porosity of porous carbons on electrochemical performance of supercapacitors, n.d. Sci. Rep. 11 (123AD) 18387. doi:10.1038/s41598-021-97932-x.
[24] A. Ahmed, S. Rafat, M. Ahmed, Nitrogen doped activated carbon derived from orange peel for supercapacitor application, Advances in Natural Sciences: Nanoscience and Nanotechnology 9 (2018), 035008, https://doi.org/10.1088/2043-6254/aad5d4.
[25] Y. Deng, Y. Xie, K. Zou, X. Ji, Review on recent advances in nitrogen-doped carbons: preparations and applications in supercapacitors, J. Mater. Chem. A Mater. 4 (2015) 1144–1173, https://doi.org/10.1039/c5ta08620e.
[26] E. Max, F. Beguin, E. Frąckowiak, Supercapacitors: Materials, Systems, and Applications, Wiley-VCH Verlag, Verlag, 2013.
[27] H. Chen, F. Yu, G. Wang, L. Chen, B. Dai, S. Peng, Nitrogen and sulfur self-doped activated carbon directly derived from elm flower for high-performance supercapacitors, ACS Omega. 3 (2018) 4724–4732, https://doi.org/10.1021/acsomega.8b00210.
[28] P. Yu, Q. Wang, L. Zheng, Y. Jiang, Construction of ultrathin nitrogen-doped porous carbon nanospheres coated with polyaniline nanorods for asymmetric supercapacitors, Front. Chem. 7 (2019) 455, https://doi.org/10.3389/fchem.2019.00455.
[29] C. Laginhas, J.M.V. Nabais, M.M. Titirici, Activated carbons with high nitrogen content by a combination of hydrothermal carbonization with activation, Microporous Mesoporous Mater. 226 (2016) 125–132, https://doi.org/10.1016/j.micromeso.2015.12.047.
[30] J. Zang, P. Tian, G. Yang, S. Jia, S. Zhou, H. Xu, Y. Wang, A facile preparation of pomegranate-like porous carbon by carbonization and activation of phenolic resin prepared via hydrothermal synthesis in KOH solution for high performance supercapacitor electrodes, Adv. Powder Technol. 30 (2019) 2900–2907, https://doi.org/10.1016/j.apt.2019.08.036.
[31] R.F. Susanti, R.G.R. Wiratmadja, H. Kristianto, A.A. Arie, A. Nugroho, Synthesis of high surface area activated carbon derived from cocoa pods husk by hydrothermal carbonization and chemical activation using zinc chloride as activating agent, Mater Today Proc. (2022), https://doi.org/10.1016/j.matpr.2022.01.042.
[32] J. Kim, J. Chun, S.G. Kim, H. Ahn, K.C. Roh, Nitrogen and fluorine co-doped activated carbon for supercapacitors, J. Electrochem. Sci. Technol. 8 (2017) 338–343, https://doi.org/10.5229/jecst.2017.8.4.338.
[33] J.R. Pels, F. Kapteijn, J.A. Moulijn, Q. Zhu, K.M. Thomas, Evolution of nitrogen functionalities in carbonaceous materials during pyrolysis, Carbon 33 (1995) 1641–1653, https://doi.org/10.1016/0008-6223(95)00154-6.
[34] J.F. Taberna, P.L. Simon, P. Fauvarque, Electrochemical characteristics and impedance spectroscopy studies of carbon-carbon supercapacitors, J Electrochem Soc. 150 (2003) A292–A300, https://doi.org/10.1149/1.1543948.
[35] A. Burke, R&D considerations for the performance and application of electrochemical capacitors, Electrochim. Acta 53 (2007) 1083–1091, https://doi.org/10.1016/j.electacta.2007.01.011.
[36] K.S.W. Sing, R.T. Williams, Physisorption hysteresis loops and the characterization of nanoporous materials, adsorptionSci. Technol. 22 (2004) 773–782, https://doi.org/10.1260/0263617053499032.
[37] Q. Gao, M.M. Titirici, Achieving high volumetric EDLC carbons via hydrothermal carbonization and cyclic activation, J. Phys. Energy 2 (2020), https://doi.org/10.1088/2515-7655/ab60e6.
[38] Q. Gao, H. Xiang, L. Ni, Y. Hou, Y. He, Z. Feng, J. Yang, W. Hu, Z. Liu, Nitrogen self-doped activated carbons with narrow pore size distribution from bamboo shoot shells, Colloids Surf. A Physicochem. Eng. Asp. 629 (2021), 127408, https://doi.org/10.1016/j.colsurfa.2021.127408.
[39] R. Arrigo, M. Ha, R. Schlo, D. Sheng Su, Dynamic surface rearrangement and thermal stability of nitrogen functional groups on carbon nanotubes, Chem. Commun. (2008) 4891–4893. www.rsc.org/chemcomm.
[40] A. Jaleel, A. Haider, C. van Nguyen, K.R. Lee, S. Choung, J.W. Han, S.H. Baek, C. H. Shin, K.D. Jung, Structural effect of nitrogen/carbon on the stability of anchored ru catalysts for CO2 hydrogenation to formate, Chem. Eng. J. 433 (2022), 133571, https://doi.org/10.1016/j.cej.2021.133571.
[41] O.Y. Podyacheva, Z.R. Ismagilov, Nitrogen-doped carbon nanomaterials: to the mechanism of growth, electrical conductivity and application in catalysis, Catal. Today 249 (2015) 12–22, https://doi.org/10.1016/j.cattod.2014.10.033.
[42] P. Sinha, A. Yadav, A. Tyagi, P. Paik, H. Yokoi, A.K. Naskar, T. Kuila, K.K. Kar, Keratin-derived functional carbon with superior charge storage and transport for high-performance supercapacitors, Carbon 168 (2020) 419–438, https://doi.org/10.1016/j.carbon.2020.07.007.
[43] Z. Zhao, S. Hao, P. Hao, Y. Sang, A. Manivannan, N. Wu, H. Liu, Lignosulphonate-cellulose derived porous activated carbon for supercapacitor electrode, J. Mater. Chem. A Mater. 3 (2015) 15049–15056, https://doi.org/10.1039/c5ta02770e.
[44] S.M. Mousavi-Khoshdel, E. Targholi, Exploring the effect of functionalization of graphene on the quantum capacitance by first principle study, Carbon 89 (2015) 148–160, https://doi.org/10.1016/j.carbon.2015.03.013.
[45] S. Ahmed, M. Rafat, A. Ahmed, Nitrogen doped activated carbon derived from orange peel for supercapacitor application, Adv. Nat. Sci. Nanosci. Nanotechnol. 9 (2018), https://doi.org/10.1088/2043-6254/aad5d4.
[46] C. Zhan, Y. Zhang, P.T. Cummings, D.E. Jiang, Enhancing graphene capacitance by nitrogen: effects of doping configuration and concentration, Phys. Chem. Chem. Phys. 18 (2016) 4668–4674, https://doi.org/10.1039/c5cp06952a.
[47] L.R. Bard, A.J. Faulkner, Electrochemical Methods: Fundamentals and Applications, John Wiley & Sons. Inc, 2001.
[48] C. Zhao, W. Zheng, A review for aqueous electrochemical supercapacitors, Front Energy Res. 3 (2015), https://doi.org/10.3389/fenrg.2015.00023.